Superconducting quantum interference device detection of acoustic nuclear quadrupole resonance of ^{121}Sb and ^{123}Sb in antimony metal

Keith S. Pickens, D. I. Bolef, M. R. Holland, and R. K. Sundfors
Laboratory for Ultrasonics, Department of Physics, Washington University, St. Louis, Missouri 63130
(Received 6 April 1984)

The acoustic nuclear quadrupole resonance (ANQR) spectra and spin-lattice relaxation times of ^{121}Sb and ^{123}Sb in antimony metal have been measured by means of the superconducting quantum interference device (SQUID) acoustomagnetic spectrometer. Novel features of the SQUID-detected ANQR spectra are described. In particular, we report the first measurement of magnetic field-dependent nuclear spin relaxation rates in a bulk metal.

I. INTRODUCTION

The high sensitivity to changes in susceptibility of the superconducting quantum interference device (SQUID) has been used to detect and study acoustic nuclear quadrupole resonance (ANQR) spectra and to measure spin-lattice relaxation times of ^{121}Sb and ^{123}Sb in single-crystal antimony metal. Measurements were made on the Zeeman-split pure quadrupole energy levels at magnetic fields between 5 and 1500 G. If one accepts the standard nomenclature for labeling these energy levels,[1,2] as shown in Fig. 1, then for convenience we may denote the transitions by the equivalent high-field energy labels, $\Delta m = \pm 1$ and $\Delta m = \pm 2$, where m is the magnetic quantum number for the nucleus with nuclear spin I. The observed resonance lines are characterized by high signal-to-noise ratios at low magnetic fields and by observed changes in magnetization whose sign depends upon the sign change in m of the transition induced, an effect not observable by non-SQUID nuclear magnetic resonance (NMR) or nuclear acoustic resonance (NAR) techniques. The measured spin-lattice relaxation rates exhibit a magnetic field dependence, the general form of which is predicted by theory.

A block diagram of the SQUID spectrometer designed to study acoustomagnetic effects in solids is shown in Fig. 2. This is the same spectrometer used by Pickens *et al.*[3] to study acoustically induced susceptibility changes in Ta metal. The spectrometer is built around a S.H.E. Co. model-SP magnetometer. As shown in Fig. 2, an astatically wound type-II superconducting pickup coil, into

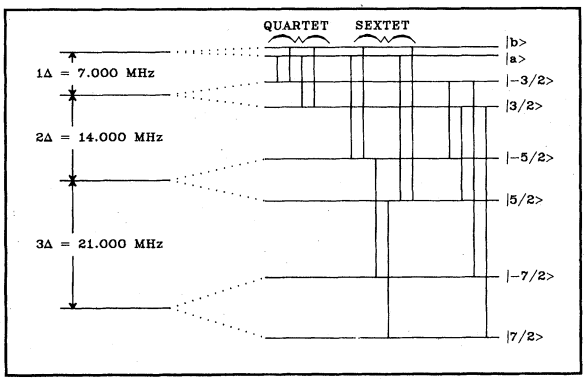

FIG. 1. Energy level configuration for ^{123}Sb with $H = 0$ (left) and $H = 500$ G (right). Spacings for $H = 500$ G are schematic. Indicated transitions have been observed for longitudinal waves ($\vec{H}||\vec{k}$) and for shear waves (the angle between $\vec{H}$ and the direction of energy propagation is 28°40′). In both cases, $\vec{H}$ is parallel to within 3.5° to the trigonal axis. The transitions labeled "quartet" refer to Fig. 3; those labeled "sextet" refer to Fig. 4.

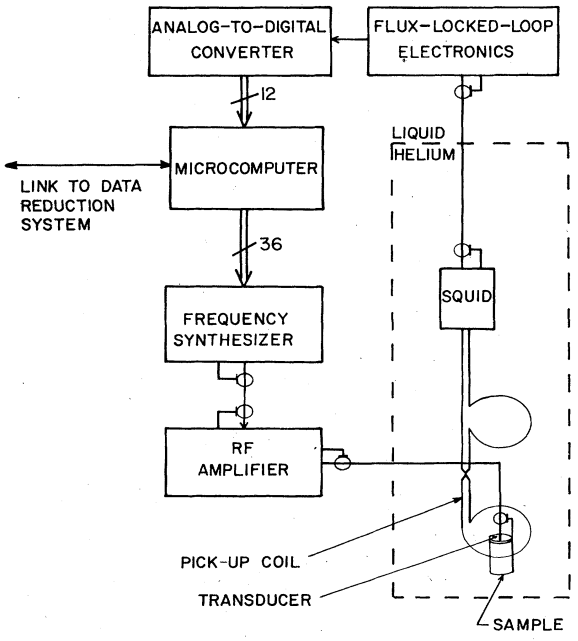

FIG. 2. Block diagram of the SQUID acoustomagnetic spectrometer with a schematic illustration showing the positions of the astatically wound type-II pickup coils and composite resonator (transducer-bond-sample). Coaxial with the pickup coils are a type-II superconducting magnet solenoid and a type-I superconducting magnetic shield.

which the sample and its holder are placed, is connected to the SQUID. A type-II superconducting, persistent-mode solenoid coaxial with the sample provides a stable magnetic field. Coaxial with the solenoid is a type-I superconductor which provides magnetic shielding. The entire probe assembly was designed and constructed by us and will be described in detail in a separate publication. Sample, SQUID, pickup coils, magnet, and shield can are placed in a common liquid-helium bath.

At resonance, the nuclear spin systems in Sb metal are driven by acoustic energy via the dynamic nuclear quadrupole mechanism as in many previous NAR experiments.[4] With the SQUID acoustomagnetic spectrometer, we observe changes in the z component of the magnetization, M_z, as the populations of the spin levels are rearranged. Changes in M_z, ΔM_z, correspond to flux changes, $\Delta\phi$, in the pickup coil, which are detected by the large flux sensitivity of the SQUID. From the decay of ΔM_z after the resonant acoustic power is removed, the spin-lattice relaxation time T_1 can be determined. Another technique used is to vary the driving frequency at approximately constant acoustic power and observe the resonance spectra, which are directly proportional to ΔM_z. Thus, the relative magnitudes and signs of ΔM_z at different resonance positions can be determined from such continuous-wave (cw) measurements. Both resonant and non-resonant acoustically induced susceptibility changes are detected with the SQUID acoustomagnetic spectrometer. The antimony single crystal has a pair of parallel faces perpendicular to the trigonal axis. We observe, with either an X- or AT-cut transducer bonded to the Sb crystal, changes in $\Delta\phi$ corresponding to mechanical resonances in the transducer frequency band-passes at the fundamental and odd harmonics.

For ^{123}Sb ($I=\frac{7}{2}$) the Zeeman-split pure quadrupole energy levels, for fields parallel to the trigonal axis, are given in Fig. 1, together with the transitions (vertical lines) observed by us in the present study. Transitions between the energy levels for ^{121}Sb ($I=\frac{5}{2}$) have also been observed by us; zero-field splittings, in this case, are given by 11.5289 MHz ($|\frac{3}{2}\rangle$ to $|\frac{1}{2}\rangle$) and 23.0611 MHz ($|\frac{5}{2}\rangle$ to $|\frac{3}{2}\rangle$).[5]

For an axially symmetric electric field gradient (EFG), as in antimony, and for the application of a weak ($\gamma\hbar H \ll e^2qQ$) constant magnetic field $\vec{H}$ at an angle θ with respect to the EFG axis (z axis), the total Hamiltonian is given by[1]

$$\mathcal{H}_{\text{op}} = \mathcal{H}_{\text{magnetic}} + \mathcal{H}_{\text{quadrupolar}} \ .$$

The energy levels for $m > \frac{1}{2}$ and for a weak magnetic field are given by[1]

$$E = \pm\gamma\hbar Hm\cos\theta + A[3m^2 - I(I+1)] \ ,$$

where

$$A = \frac{e^2qQ}{4I(2I-1)} \ ,$$

Q is the scalar quadrupole moment of the nucleus, γ is the gyromagnetic ratio, and eq is the z component of the electric field gradient.

For weak magnetic fields, mixing between the originally unsplit energy levels is negligible except in the case of $m = \pm\frac{1}{2}$, in which zero-order mixing occurs. The energy levels of Fig. 1 correspond to the case of weak Zeeman-split pure quadrupole resonance. For magnetic fields at which most of the antimony data was taken ($H \leq 500$ G) this approximation is valid; for higher fields the approximation becomes poorer and must be replaced by an exact calculation of the intermediate field energy levels, as in the NAR study of Re.[6,7]

In the present experiment, transverse and longitudinal waves were propagated along the trigonal axis of the antimony sample. The external magnetic field was also oriented along the trigonal axis corresponding to $\vec{k}\|\vec{H}$ for both longitudinal and transverse waves. For transverse waves, however, the phenomenon of internal conical refraction results in the acoustic wave energy going off at an angle with respect to the trigonal axis,[8] resulting in the beam angle being 28°40′ to $\vec{H}$.

The sample of antimony, cut from an ingot originally supplied by Monocrystals, Inc., was 1.32 cm by 1.87 cm in cross-section and 0.738 cm of thickness. The end surfaces, etched, ground, and polished to be flat and parallel to within 10^{-5} cm, were perpendicular to within 1°—2° of the trigonal axis. Seven MHz, $\frac{3}{8}$ in. diameter coaxial-plated X-cut and AT-cut transducers were bonded with silicone grease to one of the prepared faces. The transducers were driven with rf from a GR-1061 frequency synthesizer. Since the present SQUID spectrometer does not permit magnetic field sweeping, frequency was utilized as the variable to display the resonance lines. Inevitably, this introduced difficulties not ordinarily present when the more conventional magnetic field sweep is used. Thus variations in background signal and in spectrometer sensitivity as a function of frequency may be attributed to changes in acoustic response of the composite resonator (transducer-bond-sample) and to variable amplifier and transmission line responses as a function of frequency. Needless to say, strenuous attempts were made to minimize these instrumental effects.

II. EXPERIMENTAL RESULTS

Acoustic nuclear quadrupole resonance spectra of ^{121}Sb and ^{123}Sb were obtained under the following conditions: (i) transverse waves at 4.2 K and magnetic field values of $\approx$5, 147, 504, and 1467 G; (ii) longitudinal waves at 4.2 K and magnetic field values of $\approx$5, 135, and 473 G. Typical spectra are shown in Figs. 3 and 4. Figure 3 shows the ANQR spectra at $H = 504$ G for transverse waves between 6 and 8 MHz. The observed ^{123}Sb resonance lines correspond to the transitions labeled "quartet" in Fig. 1. Similarly the ^{123}Sb spectra shown in Fig. 4 correspond to the "sextet" transitions shown in Fig. 1. Correspondence between the numbered spectra in Figs. 3 and 4 and transitions of Fig. 1 is given in Table I.

In addition, most of the remaining $\Delta m = \pm 1$ and $\Delta m = \pm 2$ transitions, for transverse waves, were observed for both ^{121}Sb and ^{123}Sb. However, no $\Delta m = \pm 3$ or ± 4 transitions were observed for either isotope. For

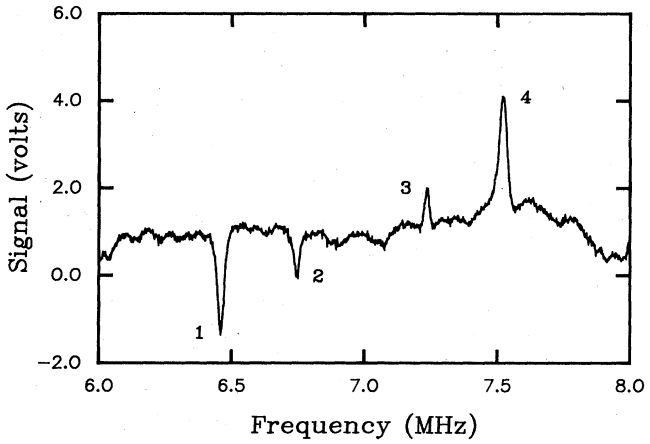

FIG. 3. ^{123}Sb NAR "quartet" at $H = 504$ G for approximately 7 MHz transverse waves with energy propagation at $\theta = 28°40'$ (due to internal conical refraction) to the trigonal axis. Notation for transitions as in Table I. The periodic structure on the baseline is due to the mechanical resonances which characterize cw acoustics in a composite resonator.

longitudinal waves the "quartet" was observed, but the "sextet" was reduced to four resonance lines, those labeled 1 and 6 not now being observed.

Spin-lattice relaxation times of both ^{121}Sb and ^{123}Sb were measured at 4.2 K for $\vec{H}$ parallel to the trigonal axis. The results for ^{123}Sb are given in Table II. The uncertainty in the measured T_1's for ^{123}Sb is estimated to be ± 0.08 sec. The signal-to-noise ratio of the ^{121}Sb lines was smaller than for ^{123}Sb since most of the ^{121}Sb transitions fell outside the frequency ranges of the 7 MHz fundamental and odd harmonics of the composite resonator. The average T_1 for ^{121}Sb at $H = 500$ G is 0.94 sec. We estimate the uncertainty of the ^{121}Sb T_1 values to be ± 0.05 sec. Within this large uncertainty, no field dependence for $T_1(^{121}\text{Sb})$ was determined.

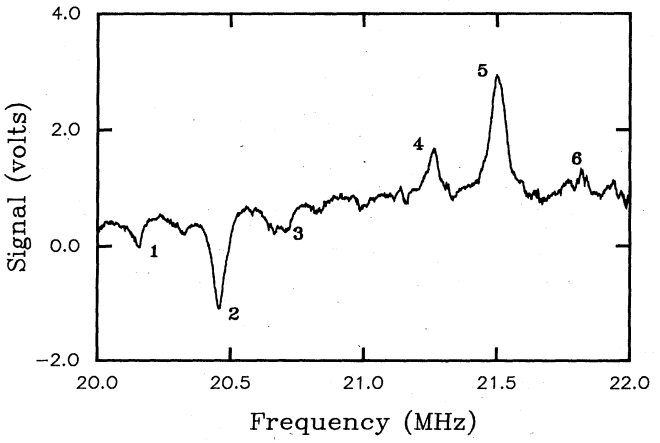

FIG. 4. ^{123}Sb NAR "sextet" with identical conditions as in Fig. 3, except the frequency is approximately 21 MHz. Notation for transitions as in Table I.

TABLE I. Transitions for ^{123}Sb: quartet and sextet.

Fig. 1	Fig. 3	Fig. 4
$\lvert -\frac{3}{2}\rangle - \lvert a\rangle$	1	
$\lvert -\frac{3}{2}\rangle - \lvert b\rangle$	2	
$\lvert +\frac{3}{2}\rangle - \lvert a\rangle$	3	
$\lvert +\frac{3}{2}\rangle - \lvert b\rangle$	4	
$\lvert -\frac{5}{2}\rangle - \lvert a\rangle$		1
$\lvert -\frac{5}{2}\rangle - \lvert b\rangle$		2
$\lvert -\frac{7}{2}\rangle - \lvert -\frac{5}{2}\rangle$		3
$\lvert +\frac{7}{2}\rangle - \lvert +\frac{5}{2}\rangle$		4
$\lvert +\frac{5}{2}\rangle - \lvert a\rangle$		5
$\lvert +\frac{5}{2}\rangle - \lvert b\rangle$		6

III. DISCUSSION

A. Dynamic coupling mechanism

The observed transitions between the levels $|a\rangle$ and $|b\rangle$, which are linear combinations, respectively, of the Zeeman states $|\frac{1}{2}\rangle$ and $|-\frac{1}{2}\rangle$ and of the levels $|\frac{5}{2}\rangle$ and $|-\frac{5}{2}\rangle$ can be attributed to the dynamic quadrupolar transitions $\Delta m = \pm 1$ and $\Delta m = \pm 2$. Despite a thorough search, no transitions corresponding to $\Delta m = \pm 3$ or $\Delta m = \pm 4$ were observed; there is therefore no need to invoke unlikely coupling mechanisms such as dynamic electric hexadecapole or dynamic magnetic octupole couplings. Dynamic dipolar (Alpher-Rubin) coupling could, for transverse waves, explain the $\Delta m = \pm 1$ transitions observed. However, the magnetization change due to dynamic dipolar coupling is proportional to H^3 and that due to dynamic quadrupole coupling to H. Therefore the theoretical ratio of $\Delta m = \pm 1$ to $\Delta m = \pm 2$ magnetization change amplitudes is field dependent if both coupling mechanisms are present; but the experimental ratio is independent of magnetic field between 5 and 500 G. We conclude that dynamic quadrupole coupling explains all of the observed transitions.

Dynamic quadrupole coupling is forbidden for longitudinal waves propagating along the trigonal axis ($\vec{k}||\vec{z}$). The observation of ANQR spectra with longitudinal waves may be explained on the basis of at least three models: (1) the coupling is so strong that the slight misorientation of 1°–2° of $\vec{k}$ to the trigonal axis is sufficient to make observation possible; (2) the Sb sample consists of two or more crystals with at least one piece oriented such that $\vec{k}$ is at a significant angle to the trigonal axis; (3) mode conversion at the crystal surfaces of longitudinal waves to transverse waves (reflected so as to propagate at an angle α to the original direction of propagation). In cases (1) and (3), the decrease in mixing for longitudinal over transverse waves, exhibited by the disappearance of lines 1 and 6 in the sextet for the longitudinal case, is explainable on the basis of $\vec{H}$ being accurately lined up along the trigonal axis. [This explanation is not consistent, however, with case (2).] We prefer to attribute the observation of ANQR spectra with $\vec{k}_{\text{long}}||\vec{z}$ to mode

conversion. That this can be an effective process has been demonstrated, for example, by Mayer,[9] who showed that for longitudinal waves incident at a very small angle δ to the plane perpendicular (due, for example, to diffraction of the acoustic beam) the reflected wave has a significant transverse component. Indeed, at $\delta \approx 3°$, the ratio of reflected to incident amplitude of the longitudinal waves is ≈ 0.5.

The $\Delta m = \pm 1$ lines can in principle also be explained as due to NMR, induced by the driving rf field at the transducer, in the electromagnetic skin-depth of the antimony sample. The obvious dependence of the observed spectra on acoustic energy density in the sample appears to minimize this possibility. Extreme care in shielding the sample from the rf field or plating the sample with a highly conductive film will be used to resolve this question. A valuable tool in furthering our understanding of the nature of the transitions, variation of angle between acoustic propagation direction and magnetic field, was not available to us with the existing probe.

B. Analysis of the observed spectra

The observed sextet of ^{123}Sb transitions in Fig. 4, for transverse acoustic wave propagation, can be explained as follows: The center positive- and negative-going lines are $\Delta m = \pm 1$ transitions between the $|\pm\frac{5}{2}\rangle$ and $|\pm\frac{7}{2}\rangle$ levels. The remaining four lines, two positive going and two negative going, can be explained as $\Delta m = \pm 2$ transitions between the $|\pm\frac{5}{2}\rangle$ levels and the $|a\rangle$ and $|b\rangle$ levels [which are linear combinations of the Zeeman states ($|\frac{1}{2}\rangle$, $|-\frac{1}{2}\rangle$), caused by a small error in sample orientation for the transverse wave case]. The measured 3.5° angle between the sample trigonal axis and the magnetic field determines the amount of mixing in the $|a\rangle$ and $|b\rangle$ levels, which qualitatively explains the $\Delta m = \pm 2$ amplitude ratios in Fig. 4.

In Fig. 3, the spectra are observed centered near the 7 MHz fundamental of the composite resonator when transverse wave propagation is used. As mentioned above, in this case, the $\Delta m = \pm 1$ and $\Delta m = \pm 2$ transitions are between the $|\pm\frac{3}{2}\rangle$ levels and the mixed levels $|a\rangle$ and $|b\rangle$.

The magnetization changes for all of the dynamic quadrupole coupling transitions have been measured to be proportional to power except at higher power where saturation effects occur.

In both Figs. 3 and 4, magnetization changes related to mechanical resonances of the composite resonator are present as a baseline distortion as frequency is swept. A future paper will discuss the origin of these "nonresonant" magnetoacoustic effects.

C. Spin-lattice relaxation times and linewidths

For $|\pm\frac{3}{2}\rangle$ to $|a\rangle$ and $|b\rangle$ transitions the observed magnetization change signals have widths at half amplitude of approximately 30 kHz for ^{121}Sb and 40 KHz for ^{123}Sb, which is in approximate agreement with the work of Hewitt and Williams[5] on Sb powders.

TABLE II. Measured ^{123}Sb T_1 values at 4.2 K for H along the trigonal axis. The experimental error is ±0.08 sec.

Transition	Frequency (MHz)	H (G)	T_1 (sec)	W_1 (sec^{-1})
$\|+\frac{3}{2}\rangle - \|b\rangle$	7.14	135	2.43	0.206
$\|+\frac{3}{2}\rangle - \|b\rangle$	7.16	147	2.48	0.202
$\|+\frac{3}{2}\rangle - \|b\rangle$	7.52	473	3.01	0.166
$\|+\frac{3}{2}\rangle - \|b\rangle$	7.56	504	2.93	0.171
$\|-\frac{3}{2}\rangle - \|b\rangle$	6.74	504	2.95	0.169
$\|+\frac{3}{2}\rangle - \|a\rangle$	7.26	504	2.86	0.175
$\|-\frac{3}{2}\rangle - \|a\rangle$	6.43	504	2.96	0.169
$\|-\frac{3}{2}\rangle - \|a\rangle$	5.36	1467	3.41	0.147

The data on ^{123}Sb nuclear spin-lattice relaxation times given in Table II indicate a magnetic field dependence of the relaxation times. To our knowledge this constitutes the first measurement of magnetic field-dependent T_1's in single-crystal metals. The theory of relaxation rates in metals, on the other hand, has been extensively treated in the literature.[10–15]

In a cubic metal the nuclear spin-lattice relaxation rate W_1 is usually taken to be the sum of the following contributions: (1) the Fermi contact interaction with conduction electrons; (2) the interaction of the nuclear magnetic moment with electron orbital moments; (3) the nuclear spin-electron spin dipolar interaction; (4) the contact interaction with closed inner shell electrons (core polarization); and (5) the electric interaction of the nuclear quadrupole moment with the electric field gradient due to the conduction electrons. The latter contribution has been calculated to be small for cubic metals,[16] although a measured value of $W_{1Q} = 1/2T_{1Q}$ of $\approx 10\%$ has been reported.[17] In the case of antimony, the work of Hewitt and MacLaughlin[18] has shown that W_{1Q} contributes approximately 2% to the total W_1. Because of the lower symmetry, for non-cubic metals the relaxation rate cannot be expressed as a simple sum of the individual contributions given above. A discussion of this more complicated situation, for hcp metals, has been given by Asada and Terakura.[15]

The magnetic field dependence of W_1 shown for ^{123}Sb in Table II indicates the same relaxation, within experimental error, for the same isotope but for different transitions. This behavior suggests that the magnetic field dependences of different transitions are quantitatively similar. Hewitt and MacLaughlin[18] have measured a constant T_1T between 4.2 and 77 K in Sb powder, which suggests that electron coupled relaxation rates dominate in Sb metal. The concept of a spin temperature cannot be applied to the situation of ANQR in Sb metal. However, one may qualitatively expect that the form of the magnetic field dependence of the conduction electron relaxation rate (derived under the concept of a spin temperature[9,10]) may apply to the field dependence of the *same* ANQR transition in Sb metal. We therefore assume the qualitative form of the field-dependent relaxation rate given by Wolf[11] to explain the measured field dependence of a single transition:

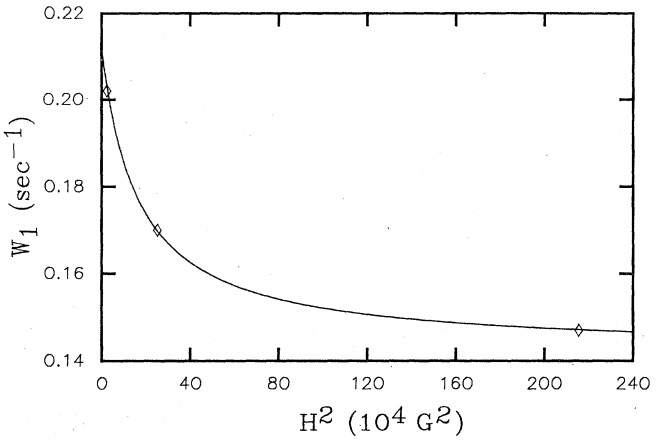

FIG. 5. Magnetic field dependence of nuclear spin relaxation rate W_1 of ^{123}Sb. The curve is the best fit of Eq. (1) to the data in Table II. The plotted data points are averages of the W_1 data at the four fields.

$$W_{1e} = W_0(H^2 + \delta H_L^2)/(H^2 + H_L^2) \ , \qquad (1)$$

where W_0 is the relaxation rate at $H \gg H_L$, and H_L is an effective "local field." The factor δ is the ratio of the zero-field relaxation rate to the high-field relaxation rate.

The W_1 data of Table II are plotted in Fig. 5 as a function of H^2. From an analysis of the fit of the equation to the data one obtains values of $\delta(^{123}\text{Sb}) = 1.49$ and of $H_L(^{123}\text{Sb}) = 410$ G. However, of major interest is the qualitative fit to the data points.

For $H = 0$ (pure quadrupole resonance) Hewitt and MacLaughlin[18] have reported values of $W_1(^{121}\text{Sb}) = 0.501\text{sec}^{-1}$ and $W_1(^{123}\text{Sb}) = 0.148$ sec^{-1}. The lack of agreement between these values and the low-field values in the present work [$W_1(^{121}\text{Sb}) = 0.59$ sec^{-1} and $W_1(^{123}\text{Sb}) = 0.21$ sec^{-1}] may be attributed to the fact that Hewitt and MacLaughlin utilized powdered samples while the present work was done on a single crystal with $\vec{H}$ oriented along the trigonal axis. As has been stated clearly by Narath,[14] the magnitudes of the non-contact contributions to W_1 in a non-cubic crystal should depend upon the orientation of the magnetic field relative to the crystal axes. We intend to investigate this anisotropy in future work.

IV. CONCLUSION

This first study in a bulk metal of acoustic nuclear quadrupole resonance in the limit of weak magnetic field ($\gamma\hbar H/A \ll 1$) demonstrates the high sensitivity of the cw SQUID acoustomagnetic technique to small changes in magnetization. At the same time, the transient SQUID technique has been used to measure novel spin-lattice relaxation effects in bulk antimony. The cw and transient SQUID acoustomagnetic techniques as used here to study ^{121}Sb and ^{123}Sb ANQR and T_1 in antimony metal can be utilized in general for the study of cw and transient acoustomagnetic effects in metals and alloys.

ACKNOWLEDGMENTS

We wish to express our appreciation to Professor P. A. Fedders for valuable discussions. Research was carried out with financial assistance of the National Science Foundation under Grant No. DMR-81-06142. One of the authors, K.S.P., acknowledges the financial support of IBM.

[1]T. P. Das and E. L. Hahn, in *Solid State Physics,* edited by F. Seitz and D. Turnbull (Academic, New York, 1958), Supplement 1.
[2]M. H. Cohen and F. Reif, in *Solid State Physics,* edited by F. Seitz and D. Turnbull (Academic, New York, 1957), Vol. 5.
[3]Keith S. Pickens, George Mozurkewich, D. I. Bolef, and R. K. Sundfors, Phys. Rev. Lett. **52**, 156 (1984).
[4]R. K. Sundfors, D. I. Bolef, and P. A. Fedders, Hyp. Int. **14**, 271 (1984).
[5]R. R. Hewitt and B. F. Williams, Phys. Rev. **129**, 1188 (1963).
[6]J. Buttet and P. K. Baily, Phys. Rev. Lett. **24**, 1220 (1970).
[7]M. Stachel and H. E. Bömmel, Appl. Phys. A **30**, 27 (1983).
[8]Seymour Epstein and A. P. De Bretteville, Jr., Phys. Rev. **138**, A771 (1965).
[9]W. G. Mayer, Ultrasonics **3**, 62 (1965).
[10]A. Abragam, *The Principles of Nuclear Magnetism* (Oxford, London, 1961).
[11]Dieter Wolf, *Spin Temperature and Nuclear Spin-Relaxation in Matter* (Clarendon, London, 1979).
[12]Y. Obata, J. Phys. Soc. Jpn. **18**, 1024 (1963).
[13]Y. Yafet and V. Jaccarino, Phys. Rev. **133A**, 1630 (1964).
[14]A. Narath, Phys. Rev. **162**, 320 (1967).
[15]T. Asada and K. Terakura, J. Phys. F **12**, 387 (1982).
[16]Y. Obata, J. Phys. Soc. Jpn. **19**, 2348 (1964).
[17]A. Narath and D. W. Alderman, Phys. Rev. **143**, 328 (1966).
[18]R. R. Hewitt and D. E. MacLaughlin, J. Magn. Reson. **30**, 483 (1978).